Postischemic treatment of neonatal cerebral ischemia should target autophagy

Julien Puyal, Anne Vaslin, Vincent Mottier, Peter G.H. Clarke

Institutions: University of Lausanne

Published on: 01 Sep 2009 - Annals of Neurology (Wiley Subscription Services, Inc., A Wiley Company)

Topics: Programmed cell death, Autophagy, Brain ischemia, Ischemia and Necrosis

Title: Postischemic treatment of neonatal cerebral ischemia should target autophagy.

Authors: Puyal J, Vaslin A, Mottier V, Clarke PG

Journal: Annals of neurology

Year: 2009 Sep

Volume: 66

Issue: 3

Pages: 378-89

DOI: 10.1002/ana.21714

Post-ischemic treatment of neonatal cerebral ischemia should target autophagy

Julien Puyal[1,2]*, PhD, Anne Vaslin[1,2], PhD, Vincent Mottier[1], and Peter G.H. Clarke[1], PhD

[1] Département de Biologie Cellulaire et de Morphologie, University of Lausanne, Switzerland.

[2] equal contribution

***Corresponding author:**

Dr Julien Puyal

Département de Biologie Cellulaire et de Morphologie (DBCM),

University of Lausanne,

Rue du Bugnon 9,

CH-1005 Lausanne,

Switzerland.

Tel: +41 21 692 5122

Fax: +41 21 692 5105

e-mail: JulienPierre.Puyal@unil.ch

Title character count: 77

Running head character count: 50

Abstract word count: 243

Body text total word count: 4469

Number of figures: 6 (4 color figures) + 3 supplementary figures

Number of references: 51

Statement of conflict of interest: none

Running title: Neonatal cerebral ischemia & autophagic cell death

Abstract

Objective: To evaluate the contributions of autophagic, necrotic and apoptotic cell death mechanisms after neonatal cerebral ischemia and hence define the most appropriate neuroprotective approach for post-ischemic therapy.

Methods: Rats were exposed to transient focal cerebral ischemia on postnatal day 12. Some rats were treated by post-ischemic administration of pan-caspase or autophagy inhibitors. The ischemic brain tissue was studied histologically, biochemically and ultrastructurally for autophagic, apoptotic and necrotic markers.

Results: Lysosomal and autophagic activities were increased in neurons in the ischemic area from 6-24h post-injury, as shown by immunohistochemistry against LAMP1 and cathepsin D, by acid phosphatase histochemistry, by increased expression of autophagosome-specific LC3-II and by punctate LC3 staining. Electron microscopy confirmed the presence of large autolysosomes and putative autophagosomes in neurons. The increases in lysosomal activity and autophagosome formation together demonstrate increased autophagy, which occurred mainly in the border of the lesion, suggesting its involvement in delayed cell death. We also provide evidence for necrosis near the centre of the lesion and apoptotic-like cell death in its border, but in nonautophagic cells. Post-ischemic intracerebro-ventricular injections of autophagy inhibitor 3-methyladenine strongly reduced the lesion volume (by 46%) even when given more than 4 hours after the beginning of the ischemia, whereas pan-caspase inhibitors, Z-VAD-fmk and Q-VD-OPH, provided no protection.

Interpretation: The prominence of autophagic neuronal death in the ischemic penumbra, and the neuroprotective efficacy of post-ischemic autophagy inhibition indicate that autophagy should be a primary target in the treatment of neonatal cerebral

ischemia.

Peri- or neonatal stroke is a major cause of brain injury and leads to serious motor and cognitive disabilities[1]. Cell death due to cerebral ischemia has generally been attributed to necrosis and apoptosis, and most research on stroke has focused on them. Attempts at neuroprotection have likewise targeted apoptosis and necrosis, particularly apoptosis, but with only limited success[2-5].

Other types of cell death exist, including autophagic, or “type 2”, cell death, characterized by numerous autophagic vacuoles. Autophagy is a physiological process by which the cell eliminates damaged organelles, toxic agents and long lived proteins by degradation in lysosomes[6]. It thus contributes to the well-being of cells, and can play a crucial pro-survival role by restoring intracellular energetic stores during nutrient deprivation. But excessive autophagy can promote cell death. Different autophagic mechanisms coexist in the same cell, but only one of them, macroautophagy (hereafter called autophagy), has been demonstrated to contribute to cell death[7-8]. In neurons, autophagy is enhanced in several conditions including nutrient starvation, development and neurodegeneration[9]. Autophagic cell death occurs in neurons during normal development and excitotoxicity[10-13] and there is increasing evidence that autophagy may be involved in mediating neuronal death in cerebral ischemia[14-17]. To develop optimal neuroprotective strategies in neonatal stroke research, it is important to understand all the cell death mechanisms involved, including autophagy.

Since more than 80% of neonatal strokes involve the middle cerebral artery[18], we here employ a model of middle cerebral artery occlusion[19]. We used P12 rats, whose brain development corresponds to that of newborn humans[1]. We show that ischemia provokes all three kinds of cell death mechanisms: apoptotic, necrotic and autophagic. Caspase inhibition was not neuroprotective, but inhibition of autophagy with 3-

methyladenine gave strong neuroprotection with a therapeutic window of at least 3h after the end of the ischemic insult, opening the way to new neuroprotective strategies in neonatal stroke research. Preliminary results have been published in abstracts[20-21].

Materials and Methods

Focal ischemia model

All animal procedures were in compliance with the directives of the Swiss Academy of Medical Science and were authorized by the veterinary office of the Canton of Vaud. Anesthesia was induced with 2.5% isoflurane in a chamber and maintained during the operation with a mask using 2.5% isoflurane. Middle cerebral artery occlusion was performed in 12 day old male Sprague-Dawley rats according to the protocol of Renolleau et al. (1998)[19] with modifications. Briefly, the main (cortical) branch of the left middle cerebral artery was electrocoagulated just below its bifurcation into frontal and parietal branches. The left common carotid artery was then occluded by means of a clip for 90min., during which time the rat pups were maintained at 37°C in the induction chamber (2.5% isoflurane). The arterial clip was then removed and the restoration of carotid blood flow was verified under a dissecting microscope before the skin incision was closed. Rat pups were transferred back to their mothers until sacrifice.

Drug administration

3-methyladenine (3-MA) was obtained from Sigma (St. Louis, MO, USA). Intra-cerebroventricular (icv) injections were performed in the contralateral ventricle with 2µl of a 30mg/ml solution prepared in saline (0.9% NaCl) or with saline alone (n=17). Rats were injected either at the beginning of reperfusion (n=9), 3h (n=7) or 6h (n=6) later.

Quinoline-Val-Asp(ome)-Ch2-O-phenoxy (Q-VD-OPh) (MP Biochemicals, Illkrich, France) was dissolved in DMSO (50mM stock solution) and further diluted with sterile PBS. Intra-peritoneal injections (ip) were performed with either 1mg/kg Q-VD-OPh (n=6) or with vehicle containing the same percentage of DMSO in PBS (phosphate-buffered saline). Another group of animals were injected icv in the contralateral ventricle at the beginning of reperfusion with 1.3µg of Q-VD-OPh, 2µl of a 1.25mM solution (n=6), prepared in PBS containing final DMSO concentration of 2.5%. Control animals were injected with 2.5% DMSO in PBS.

Carbobezoxy-Valyl-Alanyl-Aspartyl(ome)-fluoromethylketone (Z-VAD-fmk) (Sigma, St. Louis, MO, USA) was prepared as a 20mM stock solution in DMSO. Different doses of Z-VAD-fmk (500ng, n=5; 160ng, n=5; 80ng, n=8) were dissolved in 2µl of 0.9% saline and injected icv in the contralateral ventricle at the beginning of reperfusion. Control animals were treated with a saline solution containing the same percentage of DMSO.

Statistics

Normality was first tested. When the distribution was normal in all groups (experiments on caspases inhibition), one-way ANOVA was used followed by a t-test (one-tailed, unpaired). When the normality criterion was not satisfied (experiments with 3-MA), the nonparametric Kruskal-Wallis H-test was performed ($p=0.0065$) followed by a Mann-Whitney U-test (one-tailed), ($p<0.01$ for 3-MA 0h and +3h as compared with saline group and $p=0.4532$ for +6h group).

Measurement of infarct volume

Pups were heavily anesthetized with sodium pentobarbital and perfused intracardially at different times after the beginning of the reperfusion with 4% paraformaldehyde in 0.1M PBS (pH 7.4). Brains were removed, placed in PBS 30% sucrose in PBS for about 15h at 4°C and then frozen in isopentane (-40°C). Cryostat coronal sections of 50µm were stained with cresyl violet. The outline of the infarct was traced in each tenth slice using a computer-microscope system equipped with the Neurolucida program (MicroBrightField) and the infarct volume calculated with Neuroexplorer (MicroBrightField). Infarct surfaces were also plotted along the rostro-caudal axis. Animals treated with 3-MA, Q-VD-OPh and Z-VAD-fmk were sacrificed 24 hours after the beginning of reperfusion and examined as described previously.

Immunohistochemistry, electron microscopy and Western blots

The detailed experimental methods concerning immunohistochemistry, electron microscopy and Western blots are described in the Supplemental Methods section.

Histochemical staining for lysosomal enzymes

At different times following ischemia, animals were anesthetized with sodium pentobarbital (6mg/100mg body weight, ip) and perfused intracardially with 2% glutaraldehyde and 1% paraformaldehyde diluted in cacodylate buffer (0.1M, pH 7.4). Brains were removed and post-fixed in the same fixative solution overnight at 4°C, then washed three times in 0.1M cacodylate buffer (pH 7.3). Coronal vibratome sections (30-50µm thick) were done cut and stained as described below.

Acid phosphatase histochemistry - Coronal brain sections were treated for acid phosphatase histochemistry with several modifications of Gomori's sodium β-glycerophosphatase method[22]. Briefly, after several washes in distilled water, sections were incubated for 2h at 37 °C in 0.01M Na-β-glycerophosphate and 8 µM lead nitrate in sodium acetate buffer (50mM, pH 5). The incubation solution had been filtrated before use and was kept for 1h at 37 °C. After incubation, sections were rinsed in distilled water and immersed in ammonium sulphide (0.5%) for 30s, rinsed again and mounted in fluorsave. Controls were performed using sodium fluoride to verify the labeling specificity. No staining was detected in any of these controls.

β-N-acetylhexosaminidase histochemistry - The histochemical method for β-hexosaminidase was performed as previously described[23]. Briefly, sections were washed in distilled water and then incubated for 1h at 37 °C in Fast red violet salt solution (0.63M ethylene glycol monomethyl ether, 1% polyvinyl pyrrolidone, 0.1M citric acid-citrate buffer pH 4.4, 1.6M sodium chloride, 2.7mM Fast red violet LB salt (Sigma)) using 0.5mM Naphthol-AS-BI-N-acetyl-β-D-glucosaminide (Sigma) as the substrate. Then, sections were rinsed in distilled water and fixed for 10min in 10% formaldehyde. After post-fixation the sections were rinsed twice with distilled water, dehydrated in graded alcohol and mounted in Eukitt medium. To verify the staining specificity, controls without the substrate or at basic pH were done in parallel. No staining was detected in any of these controls.

Results

We first characterized the brain lesion obtained using a model of focal cerebral ischemia adapted from Renolleau et al. (1998)[19] in P12 rats (see supplementary results). The resulting lesion was restricted to the ipsilateral cortex and reached its maximum volume at 24h post-ischemia (see suppl. Fig S1).

Then, in order to develop a relevant neuroprotective approach, we analyzed the different cell death mechanisms involved in the ischemic brain damage.

Early necrosis at the center of the lesion

Evidence for necrosis was demonstrated by electron microscopy and by Western blot for calpain-dependent fodrin cleavage, previously used as a marker of necrosis following cerebral ischemia[24] (see Suppl. Fig S2). In this model, necrosis occurred rapidly and was mainly located at the center of the lesion (see Supplementary Results).

Evidence for apoptotic mechanisms

Electron microscopy revealed dying neurons with some apoptotic features in the border of the lesion. These neurons did not display classical criteria of apoptosis but did present chromatin condensation (although more irregular and fragmented than in classical apoptosis), cytoplasm shrinkage, and relatively good preservation of cytoplasmic organelles (slightly swollen) such as mitochondria in the border of the lesion (Fig 1A).

We then assessed the occurrence of caspase-dependent and apoptosis-inducing factor (AIF)-dependent apoptotic mechanisms. Western blot using a specific antibody against cleaved (activated) caspase-3 showed no detectable cleavage in the control condition, but a significant increase in cleavage from 6h post-reperfusion that increased progressively to reach its maximum value at 24h (Fig 1B). Caspase-3 dependent fodrin breakdown (Fig 1C) was likewise significantly increased from 6h (189% ± 21) to 24h (469% ± 84) (Suppl. Fig S2). By immunocytochemistry, we investigated the expression and cellular distribution of active caspase-3 and -9 at 24h post-reperfusion using antibodies that recognized only their activated forms. Cleaved caspase-3 (Fig 1C, arrows) and -9 (Fig 1F, arrows) were both detected mainly in the border of the lesion. Double labeling using both neuronal and glial markers demonstrated that cleaved caspase-3 (Fig 1D, E) and -9 (Fig 1G, H) were mainly colocalized with the neuronal marker NeuN (Fig 1D, G, arrowheads) and that no colocalizations were detected with the glial marker GFAP (Fig 1E, H).

We then investigated whether the caspase-independent component of apoptosis was implicated, focusing on AIF (apoptosis-inducing factor), which is released from the mitochondria and translocated to the nucleus, where it is involved in DNA fragmentation. Immunocytochemistry showed a cytosolic distribution of AIF in control conditions (Fig 1I) but a nuclear localization in the ischemic area after cerebral ischemia (Fig 1J), suggesting the involvement of AIF-mediated caspase-independent apoptotic mechanisms.

Attempts at neuroprotection using caspase inhibitors

As apoptotic mechanisms appear to be strongly involved in our model, we investigated the effects of two broad-band caspase inhibitors, Z-VAD-fmk and Q-VD-OPH (Fig 1K-N). We first verified that Z-VAD-fmk and Q-VD-OPH both strongly inhibited caspase-3 activation (Figs 1K and 1M, respectively). Then, we evaluated the effect of both inhibitors on the infarct volume. Different doses of Z-VAD-fmk were administered icv at the moment of reperfusion (Fig 1L), but none of them significantly reduced the infarct volume as compared to the saline-treated group. Similarly, two modes of injection of QVD-OPH were tested (Fig 1N), but neither icv nor ip injections (at the moment of reperfusion) significantly reduced the lesion volume as compared to saline injected rats.

Involvement of autophagy after neonatal cerebral ischemia in P12 rats

In view of the lack of neuroprotection using caspase inhibitors, we investigated whether autophagic cell death mechanisms were contributing to ischemic brain damage.

Increase in autophagosomes. To evaluate the involvement of autophagosomes, we used electron microscopy, Western blots and immunocytochemistry. Western blot analyses were performed using an antibody against LC3 (microtubule-associated protein 1A light chain 3). LC3 is distributed in the cytoplasm in normal conditions (LC3-I), but when autophagy is induced, LC3 is modified post-translationally to become LC3-II, which integrates the autophagosome membrane. Quantification of LC3-II was done to determine the level of autophagosomes in the ischemic cortex from 0h to 24h after the moment of reperfusion. LC3-II levels increased about 2.5-fold between 2h and 6h post-ischemia, followed by a moderate further increase up to 24h (Fig 2A).

Immunocytochemistry using an anti-LC3 antibody revealed at 24h the presence of numerous cells showing a strong LC3-positive staining (Fig 2D). At higher magnification (Fig 2E), the labeling in these highly reactive neurons displayed numerous positive dots, presumably autophagosomes, which was quite unlike the diffuse staining seen in LC3-positive cells in control animals (Fig 2B, C). Double labeling experiments revealed that LC3 is expressed selectively in neurons, as shown by numerous colocalizations with NeuN (Fig 2F) in contrast to the absence of colocalization with glial fibrillary acidic protein (GFAP) (Fig 2G) or other glial markers such as S100β (not shown). At 24h (Fig 2H), electron microscopy revealed in the border of the lesion neurons containing numerous autophagosome-like structures filled with amorphous material (arrows) and autolysosomes filled with membranous whorls (arrowheads).

Studies on the lysosomal pathway

To clarify whether the increase in autophagosomes reflected an increase in autophagic activity (or flux) or a decrease in their turnover, we also investigated the activity of the lysosomal pathway. First, we performed immunocytochemistry against the lysosomal protease cathepsin D, and the lysosomal-associated membrane protein 1 (LAMP1), to investigate lysosomal expression and to characterize their cellular distribution (Fig 3). Already at 6h after reperfusion, an increase in the number of cathepsin D-positive dots was observed in cells located mainly in the border in the lesion (Fig 3B, B'). At 24h, a further increase in the intensity and size of the cathepsin D labeling was detected as compared to 6h (Fig 3C, C'). At 24h, double labeling using NeuN for neurons and several glial markers demonstrated that numerous cells strongly immunoreactive for cathepsin D are neurons (Fig 3D-D', white arrows) whereas no colocalizations were obtained between cathepsin D and glial markers such as GFAP (Fig 3E, E') and S100β (not shown).

LAMP1 immunostaining likewise increased strongly in the ischemic hemisphere from 6h (Fig 3G, G') to 24h (Fig 3H, H') post-reperfusion as compared to control cortex (Fig 3F, F'). At 24h, double labeling with microtubule-associated protein 2 (MAP2) revealed that the cells displaying intense LAMP1 labeling are neurons (Fig 4I'') and not glial cells (Fig 5J'').

Histochemistry directed against two lysosomal hydrolases, acid phosphatase and β-N-acetylhexosaminidase, showed a strong increase in lysosomal activity from 6h. As shown in figure 4, acid phosphatase staining is enhanced (number and size of acid phosphatase positive dots) in neurons mainly in the border of the lesion from 6h (Fig 4B, B') to 24h (Fig 4C, C') compared to control cortex (Fig 4A, A'). The dots presumably show lysosomes, and the larger dots autolysosomes[13].

β-N-acetylhexosaminidase staining is likewise strongly increased in neurons located in the border of the ischemic area from 6h (Fig 4E, E') to 24h (Fig 4F, F') post-ischemia compared to the control cortex (Fig 4D, D'). Again, both the number and the size of the reactive regions, presumably lysosomal, is increased.

Relationship between lysosomal and autophagosomal pathways

Double labeling at 24h post-reperfusion showed that the strong punctate autophagosomal labeling (LC3) and the strong lysosomal labeling (cathepsin D and LAMP1) are in the same neurons (Fig 4). Numerous colocalizations can be seen between LC3 and cathepsin D (Fig 4G''), or between LC3 and LAMP1 (Fig 4H'').

Relationship between autophagic and apoptotic mechanisms

Double labeling was performed to investigate the relationship between autophagic and apoptotic mechanisms (see supplementary Fig S3). Neurons positive for cleaved caspase-3 (Fig S3A, D) were never strongly labeled for LAMP1 (Fig S3A'') or cathepsin D (Fig S3D'') and tended not to occur in the same region as the LAMP1 (Fig S3B') or cathepsin D (Fig S3C') positive neurons. The same approach revealed no colocalizations between cleaved caspase-9 and LAMP1 (Fig S3E'', F'') or cathepsin D (Fig S3G'', H'').

Neuroprotective effect of 3-methyladenine against neonatal cerebral ischemia

We used 3-methyladenine (3-MA), a pharmacological inhibitor of autophagy, to investigate the functional significance of the increase in autophagy (Fig 5). First, we evaluated the capacity of 3-MA to down-regulate the ischemia-induced increase in LC3-II. Western blot analyses of ischemic extracts collected 24h after icv injections of 3-MA showed a strong and highly significant ($p<0.01$) decrease in LC3-II levels compared to saline-treated animals (Fig 5A). Then, we examined whether the autophagy inhibitor could provide neuroprotection in our ischemic model. Four groups of P12 rats received an icv injection of either saline or of 3-MA (60µg) at different time points after the beginning of reperfusion (Fig 5B). When given at the moment of reperfusion, 3-MA provided more than 37% of neuroprotection (Fig 5C) in terms of lesion volume evaluated by measurement of pale cresyl violet staining, and compared to ischemic rats injected with saline (Fig 5D). In view of this strong neuroprotective effect, we investigated the post-ischemic therapeutic window of 3-MA by testing later icv injections of 3-MA. Even stronger neuroprotection (>46%) was obtained with 3-MA given at 3h but not at 6h after reperfusion. We also evaluated the neuroprotective effect of 3-MA along the antero-posterior axis, and found that 3-MA treatment at 0h (Fig 5E) or at 3h (Fig 5F) was in both cases more neuroprotective in the more caudal part of the cortex, corresponding mainly to the region where delayed cell death was most prominent (level of the hippocampus, see supplementary Fig S1).

Relationship between 3-MA treatment and nonautophagic cell death mechanisms

We investigated the effect of blocking autophagy on nonautophagic modes of cell death (Fig 6). Western blots of 3-MA-treated ischemic cortex showed that 3-MA caused a strong and significant decrease in cleaved caspase-3 levels. As shown in Fig 8A, 3-MA treatment significantly reduced, by 70.6%, the activation of cleaved caspase-3 as compared to saline controls. 3-MA also decreased significantly, by 54.9%, the caspase-specific fodrin cleavage product as compared to saline controls (Fig 6B). However, 3-MA treatment did not significantly reduce the calpain-specific fodrin cleavage product (Fig 6B).

We also counted the caspase-9-positive cells in sections through the ischemic cortex of rats treated with 3-MA or saline (Fig 6C). In rats treated with 3-MA there was a strong reduction (by 72%) in the density of caspase-9 positive cells with respect to the saline-treated rats.

We then investigated the effect of 3-MA on AIF translocation to the nucleus (Fig 6D). Counts of positive AIF nuclei at 24h of reperfusion revealed a 60.1% reduction as compared to the saline control, indicating that 3-MA strongly decreased the ischemia-induced translocation of AIF.

Discussion

We here report that neonatal cerebral ischemia caused early neuronal death occurring by necrosis in the centre of the lesion, followed by delayed neuronal death involving apoptotic and autophagic mechanisms at the border of the lesion. Post-ischemic autophagy inhibition was strongly neuroprotective whereas caspase inhibition was not.

Necrosis and apoptosis

As expected from previous studies on both adults and neonates[14, 19, 24-28], cerebral ischemia in P12 rats induced both necrotic and apoptotic-like neuronal death. Necrosis occurred early after the ischemic insult and was restricted to the center of the lesion as deduced from both ultrastructure and the activation of calpain, a mediator of necrotic cell death[24]. Apoptotic-like cell death occurred later and was restricted to the border of the lesion. Neonatal cerebral ischemia strongly activated caspases-3 and -9 in neurons in the penumbra, as reported in other neonatal and adult models[3, 28-29] and also induced AIF nuclear translocation, shown to occur after neonatal hypoxia-ischemia[29-31], demonstrating that both caspase-dependent and -independent components of apoptosis are involved in delayed neuronal death in the present model.

Post-ischemic inhibition of caspase activation is not neuroprotective

In view of the inhomogeneous potency profiles of so called “pan-caspase” inhibitors[32], we tested both Z-VAD-fmk (the most widely used pan-caspase inhibitor) and Q-VD-OPh (more potent than Z-VAD-fmk, especially for caspases-2 and -6), but neither reduced the lesion volume at the doses used (icv and ip), despite the fact that cerebral levels of cleaved-caspases were strongly reduced by both inhibitors. The reason for this is not known. Previous studies with pan-caspase inhibitors have shown protection in various models ranging from neonatal cerebral hypoxia-ischemia[2, 29, 31] and focal cerebral ischemia[5] to adult focal cerebral ischemia. However, there are also reports of a lack of protection in these same models (e.g. neonatal cerebral hypoxia-ischemia[3] and focal cerebral ischemia[4]). Various factors may have contributed to the discrepancies including the sex of the animals[5, 30-31], the time of caspases inhibitor administration, the severity of the ischemic insult and the differences between the models used. The present data suggest that the resistance to treatment may be due to the activation of multiple cell death pathways, with the result that inhibiting caspases alone may be insufficient for protection. For this reason we hypothesized that it would be necessary to target additional death pathways such as the autophagic pathway.

Neonatal focal cerebral ischemia-induced autophagy

Autophagic activity is enhanced in dying neurons in hippocampal organotypic slices exposed to an excitotoxic dose of NMDA[13], in hippocampal neurons following kainate injections[12, 33] and in motor neurons in a model of slow glutamate excitotoxicity in vitro[34]. Recently, several studies mentioned the involvement of autophagy following cerebral ischemia in both adult and neonatal models[15-17, 24, 30, 35-36]. Some of them indicated that autophagy could be implicated in mediating cell death[17, 36] but more investigations are needed to clarify this.

To demonstrate that autophagic mechanisms are increased it is not sufficient to show an increase in the number of autophagosomes or an increased expression of LC3-II, because these changes could be caused merely by a slower elimination of autophagosomes due to a reduction in lysosomal activity or a defect in autophagosome-lysosome fusion. Previous studies on other models of cerebral ischemia showed increases in autophagosomal markers[29, 16-17, 36] or in lysosomal protease activities[37-39]. We here demonstrated that the increases occurred in both autophagosomal and lysosomal markers and that both occurred in the same stressed neurons, providing unequivocal evidence that the autophagosomal increases were not due to a reduction in lysosomal activity. The alternative possibility of a defect in autophagosome-lysosome fusion can also be rejected because our ultrastructural observations showed that autolysosomes (created by autophagosome-lysosome fusion) were far more abundant in the ischemic area than in control tissue. Hence one can conclude that autophagic activity (i.e. flux) was indeed increased. In view of the autophagic neurons' location in the border of the lesion, the enhanced autophagy could be implicated in mediating the delayed neuronal death.

Post-ischemic autophagy inhibition promotes strong neuroprotection

Very recent studies have suggested that autophagy could be implicated in neuronal death following cerebral ischemia. Wen et al.[36] reported that 3-MA could promote moderate neuroprotection in adult focal cerebral ischemia. Koike et al.[17] described strongly enhanced autophagy following hypoxia-ischemia in both neonatal and adult mice, and showed that deletion of Atg7 protected hippocampal pyramidal neurons in the neonates. Nevertheless, to date no study has reported neuroprotection due to post-ischemic inhibition of autophagy.

Having provided evidence that ischemia triggers an enhanced autophagic flux, we tested the effects of inhibiting autophagy with 3-MA. Despite its potential proapoptotic side effects due to inhibition of the anti-apoptotic phosphatidylinositol 3-phosphate kinase/Akt pathway, 3-MA treatment was strongly neuroprotective, reducing the lesion volume by 37%. Furthermore, 3-MA was strongly protective (by 46%) even when given 3h after the end of the ischemic insult (i.e more than 4h after the beginning of the ischemia). Taken together, these results indicate that delayed neuronal death mechanisms may be mediated by enhanced autophagy, suggesting a therapeutic potential of autophagy inhibition in neonatal stroke.

Energy-dependence of cell death

It is widely accepted that apoptosis and autophagy are energy-dependent and that energy failure causes necrosis, although it is not clear whether the necrotic nature of this cell death is due solely to the failure of apoptosis and autophagy, or whether it is due also to other factors such as the faster demolition rate by necrotic mechanisms following massive calcium influx in energy-deprived cells. In focal cerebral ischemia it is generally accepted that apoptosis tends to occur late and at the border of the ischemic area, whereas necrosis occurs earlier and at the centre[40, 41]. Since autophagy is energy-dependent, one would expect autophagy-expressing cell death to occur likewise in the border region; as had previously been reported in an ultrastructural study of transient focal ischemia in adults[42], and our present results provide strong confirmation. There is also evidence for a *continuum* of neuronal death morphology in which gradual transitions from necrotic to necrotic-apoptotic to apoptotic morphologies occur along a temporal or spatial gradient, and this has been attributed to a corresponding energy gradient[25, 43-46]. The question arises therefore whether autophagy-expressing neuronal death can fit into such a scheme, and the above-cited work of Aggoun-Zouaoui[42] does provide some support for a gradient from necrosis at the lesion centre to apoptosis at its extreme border with autophagy-expressing neuronal death between the two.

Relationship between autophagic and apoptotic mechanisms

To clarify whether the effects of 3-MA involved interactions with nonautophagic pathways, we investigated its effect on necrotic (calpain) and apoptotic (caspases and AIF) markers. It had no effect on calpain activation, but decreased caspase activation and AIF nuclear translocation, indicating that it inhibited both the caspase-dependent and -independent apoptotic pathways. Apoptosis and autophagy are morphologically different types of programmed cell death, and can function independently, but numerous interactions between these two pathways have been described, and modifications of the autophagic pathway can influence apoptosis[7-8, 47-48]. Indeed calpain-mediated cleavage of Atg5 was demonstrated to mediate a switch from autophagy to apoptosis[48]. Excessive autophagy (by overexpression of Atg1) can induce apoptotic cell death[49] and several reports concerning neurons mentioned the involvement of autophagy before apoptosis following an apoptotic stimulus such as nerve growth factor deprivation in sympathetic neurons[50], chloriquine treatment in cortical neurons[51], or low-potassium induced apoptosis in cultured cerebellar granule cells[11]. Other studies have demonstrated that both autophagy and apoptosis can occur within the same cells. Indeed Rami et al.[16] showed colocalizations between caspase-3 and increased beclin-1 expression following focal cerebral ischemia in adult rats. Another recent study also showed that 3-MA was able to reverse the apoptotic death of rat striatal neurons induced by kainic acid[33]. In the work of Koike et al.[17], the apoptotic pathway (caspase-3 activation and DNA fragmentation) was inhibited by Atg7 deficiency in the hippocampus after neonatal HI. Thus, autophagy can contribute to programmed cell death by activating the apoptotic pathway.

Nevertheless, in our study activated caspase-3/9 never colocalized with the strong LAMP1 or cathepsin D immunolabelling, suggesting that the apoptotic and autophagic processes occurred in different neurons or at different times in the same neurons. We obtained a similar lack of colocalization in double-labeling experiments for LC3 and TUNEL (data not shown). Interestingly neurons displaying either strong autophagic features or caspase activation were located in the border of the lesion where delayed cell death occurs. While it is true that 3-MA reduced caspase-3 activation, this was probably not the main cause of the protection, because pan-caspase inhibitors did not provide any neuroprotective effect. In a study on chloriquine-induced neuronal death, which displayed autophagic features, 3-MA was protective whereas pan-caspase inhibitors were not[51].

We therefore hypothesize that autophagy may mediate neuronal death in our neonatal stroke model by acting in two different ways: by triggering apoptosis (via caspase-mediated and AIF-mediated pathways), and independently of apoptosis by a pure autophagic death pathway. The relevance of this to other models such as the neonatal hypoxia-ischemia model of cerebral asphyxia remains to be determined and will be the subject of another study.

Conclusion

In conclusion, we here provide evidence for a major involvement of autophagy in mediating neuronal death following focal cerebral ischemia in neonatal rats. We also report for the first time the neuroprotective effects of an autophagy inhibitor administered after the insult, opening new therapeutic possibilities.

Acknowledgments

We thank Sonia Naegele-Tollardo, Vanessa Waechter, Coralie Rummel and Kirsi Bourget for technical assistance, Jean-Yves Chatton and Yannick Krempp of the Cellular Imaging Facility (University of Lausanne) for experimental support, and the Centre of Electron Microscopy at the University of Lausanne for the use of their electron microscopes. This research was supported by grants from the Swiss National Science Foundation (3100A0-101696 and -113925) and from the Fondation Motrice.

Supplementary information is available at *Annals of Neurology*'s website.

References

1. Ferriero DM. Neonatal brain injury. N Engl J Med 2004;351:1985-95.
2. Cheng Y, Deshmukh M, D'Costa A et al. Caspase inhibitor affords neuroprotection with delayed administration in a rat model of neonatal hypoxic-ischemic brain injury. J Clin Invest 1998;101:1992-9.
3. Gill R, Soriano M, Blomgren K et al. Role of caspase-3 activation in cerebral ischemia-induced neurodegeneration in adult and neonatal brain. J Cereb Blood Flow Metab. 2002;22:420-30.
4. Joly LM, Mucignat V, Mariani J et al. Caspase inhibition after neonatal ischemia in the rat brain. J Cereb Blood Flow Metab 2004;24:124-31.
5. Renolleau S, Fau S, Goyenvalle C et al. Specific caspase inhibitor Q-VD-OPh prevents neonatal stroke in P7 rat: a role for gender. J Neurochem 2007;100:1062-71.
6. Shintani T, Klionsky DJ. Autophagy in health and disease: a double-edged sword. Science 2004;306:990-5.
7. Shimizu S, Kanaseki T, Mizushima N et al. Role of Bcl-2 family proteins in a non-apoptotic programmed cell death dependent on autophagy genes. Nat Cell Biol 2004;6:1221-8.
8. Yu L, Alva A, Su H et al. Regulation of an ATG7-beclin 1 program of autophagic cell death by caspase-8. Science 2004;304:1500-2.
9. Nixon RA. Autophagy in neurodegenerative disease: friend, foe or turncoat? Trends Neurosci 2006;29:528-35.

10. Clarke PGH. Developmental cell death: morphological diversity and multiple mechanisms. Anat Embryol (Berl) 1990;181:195-213.

11. Canu N, Tufi R, Serafino AL et al. Role of the autophagic-lysosomal system on low potassium-induced apoptosis in cultured cerebellar granule cells. J Neurochem 2005;92:1228-42.

12. Shacka JJ, Lu J, Xie ZL et al. Kainic acid induces early and transient autophagic stress in mouse hippocampus. Neurosci Lett 2007;414:57-60.

13. Borsello T, Croquelois K, Hornung JP, Clarke PGH. N-methyl-d-aspartate-triggered neuronal death in organotypic hippocampal cultures is endocytic, autophagic and mediated by the c-Jun N-terminal kinase pathway. Eur J Neurosci 2003;18:473-85.

14. Nitatori T, Sato N, Waguri S et al. Delayed neuronal death in the CA1 pyramidal cell layer of the gerbil hippocampus following transient ischemia is apoptosis. J Neurosci 1995;15:1001-11.

15. Adhami F, Liao G, Morozov YM et al. Cerebral ischemia-hypoxia induces intravascular coagulation and autophagy. Am J Pathol 2006;169:566-83.

16. Rami A, Langhagen A, Steiger S. Focal cerebral ischemia induces upregulation of Beclin 1 and autophagy-like cell death. Neurobiol Dis 2008; 29:132-41.

17. Koike M, Shibata M, Tadakoshi M et al. Inhibition of autophagy prevents hippocampal pyramidal neuron death after hypoxic-ischemic injury. Am J Pathol 2008;172:454-69.

18. Ashwal S, Pearce WJ. Animal models of neonatal stroke. Curr Opin Pediatr 2001;13:506-16.

19. Renolleau S, Aggoun-Zouaoui D, Ben-Ari Y, Charriaut-Marlangue C. A model of transient unilateral focal ischemia with reperfusion in the P7 neonatal rat: morphological changes indicative of apoptosis. Stroke 1998;29:1454-60.

20. Puyal J, Vaslin A, Waechter V et al. Autophagic cell death and transient focal cerebral ischemia in neonatal rats. FENS Abstr 2006;3: A132.27.

21. Puyal J, Vaslin A, Bourget K et al. Autophagy mediates neuronal death in neonatal cerebral ischemia: a new target for neuroprotection? 2007;8e Colloque de la Société des neurosciences, A3O.

22. Gömöri G. Distribution of acid phosphatase in tissues under normal and under pathologic conditions. Arch Path 1941;32:189-199.

23. Katayama Y, Kobatake H, Shida H. A modified technique of histochemical demonstration for N-acetyl-β-hexosaminidase. Acta Histochem Cytochem 1976;9:111-124.

24. Zhu C, Wang X, Xu F et al. The influence of age on apoptotic and other mechanisms of cell death after cerebral hypoxia-ischemia. Cell Death Differ 2005;12:162-76.

25. Northington FJ, Ferriero DM, Graham EM et al. Early Neurodegeneration after Hypoxia-Ischemia in Neonatal Rat Is Necrosis while Delayed Neuronal Death Is Apoptosis. Neurobiol Dis 2001;8:207-19.

26. Liu CL, Siesjö BK, Hu BR. Pathogenesis of hippocampal neuronal death after hypoxia-ischemia changes during brain development. Neuroscience 2004;127:113-25.

27. Renolleau S, Benjelloun N, Ben-Ari Y, Charriaut-Marlangue C. Regulation of apoptosis-associated proteins in cell death following transient focal ischemia in rat pups. Apoptosis 1997;2:368-76.

28. Benjelloun N, Joly LM, Palmier B et al. Apoptotic mitochondrial pathway in neurones and astrocytes after neonatal hypoxia-ischaemia in the rat brain. Neuropathol Appl Neurobiol 2003;29:350-60.

29. Zhu C, Qiu L, Wang X et al. Involvement of apoptosis-inducing factor in neuronal death after hypoxia-ischemia in the neonatal rat brain. J Neurochem 2003;86:306-17.

30. Zhu C, Xu F, Wang X et al. Different apoptotic mechanisms are activated in male and female brains after neonatal hypoxia-ischaemia. J Neurochem 2006;96:1016-27.

31. Zhu C, Wang X, Huang Z et al. Apoptosis-inducing factor is a major contributor to neuronal loss induced by neonatal cerebral hypoxia-ischemia. Cell Death Differ 2007;14:775-84.

32. Chauvier D, Ankri S, Charriaut-Marlangue C et al. Broad-spectrum caspase inhibitors: from myth to reality? Cell Death Differ 2007;14:387-91.

33. Wang Y, Han R, Liang ZQ et al. An autophagic mechanism is involved in apoptotic death of rat striatal neurons induced by the non-N-methyl-D-aspartate receptor agonist kainic acid. Autophagy 2008;4;214-26.

34. Matyja E, Taraszewska A, Nagańska E et al. Autophagic degeneration of motor neurons in a model of slow glutamate excitotoxicity in vitro. Ultrastruct Pathol 2005;29:331-9.

35. Erlich S, Shohami E, Pinkas-Kramarski R. Neurodegeneration induces upregulation of Beclin 1. Autophagy 2006;2:49-51.

36. Wen YD, Sheng R, Zhang LS et al. Neuronal injury in rat model of permanent focal cerebral ischemia is associated with activation of autophagic and lysosomal pathways. Autophagy 2008;4:762-9.

37. Uchiyama Y. Autophagic cell death and its execution by lysosomal cathepsins. Arch Histol Cytol 2001;64:233-46.

38. Nitatori T, Sato N, Kominami E, Uchiyama Y. Participation of cathepsins B, H, and L in perikaryal condensation of CA1 pyramidal neurons undergoing apoptosis after brief ischemia. Adv Exp Med Biol 1996;389:177-85.

39. Kohda Y, Yamashima T, Sakuda K et al. Dynamic changes of cathepsins B and L expression in the monkey hippocampus after transient ischemia. Biochem Biophys Res Commun 1996;228:616-22.

40. Ferrer I. Apoptosis: future targets for neuroprotective strategies. Cerebrovasc Dis 2006;21 Suppl 2:9-20.

41. Doyle KP, Simon RP, Stenzel-Poore MP. Mechanisms of ischemic brain damage. Neuropharmacology 2008;55:310-8.

42. Aggoun-Zouaoui D, Margalli I, Borrega F et al. Ultrastructural morphology of neuronal death following reversible focal ischemia in the rat. Apoptosis 1998;3:133-41.

43. Portera-Cailliau C, Price DL, Martin LJ. Non-NMDA and NMDA receptor-mediated excitotoxic neuronal deaths in adult brain are morphologically distinct: further evidence for an apoptosis-necrosis continuum. J Comp Neurol 1997;378(1):88-104.

44. Portera-Cailliau C, Price DL, Martin LJ. Excitotoxic neuronal death in the immature brain is an apoptosis-necrosis morphological continuum. J Comp Neurol 1997;378(1):70-87.

45. Northington FJ, Zelaya ME, O'Riordan DP et al. Failure to complete apoptosis following neonatal hypoxia-ischemia manifests as "continuum" phenotype of cell

death and occurs with multiple manifestations of mitochondrial dysfunction in rodent forebrain. Neuroscience 2007;149(4):822-33.

46. Blomgren K, Leist M, Groc L. Pathological apoptosis in the developing brain. Apoptosis 2007;12:993-1010.
47. Boya P, González-Polo RA, Casares N et al. Inhibition of macroautophagy triggers apoptosis. Mol Cell Biol 2005;25:1025-40.
48. Yousefi S, Perozzo R, Schmid I et al. Calpain-mediated cleavage of Atg5 switches autophagy to apoptosis. Nat Cell Biol 2006;8:1124-32.
49. Scott RC, Juhász G, Neufeld TP. Direct induction of autophagy by Atg1 inhibits cell growth and induces apoptotic cell death. Curr Biol 2007;17:1-11.
50. Xue L, Fletcher GC, Tolkovsky AM. Autophagy is activated by apoptotic signalling in sympathetic neurons: an alternative mechanism of death execution. Mol Cell Neurosci 1999;14:180-98.
51. Zaidi AU, McDonough JS, Klocke BJ et al. Chloroquine-induced neuronal cell death is p53 and Bcl-2 family-dependent but caspase-independent. J Neuropathol Exp Neurol 2001;60:937-45.

Figure Legends

Figure 1: Involvement of apoptosis following cerebral ischemia at P12.

(A) Electron microscopy micrograph showing a dying neuron with some apoptotic features in the border of the lesion at 24h post-reperfusion. Note the chromatin condensation in the nucleus (n) and the cytoplasmic shrinkage (dark cytoplasm). **(B)** Representative cleaved caspase-3 immunoblot of ischemic cortex homogenates after 0h, 2h, 6h, 12h and 24h of reperfusion. Quantification of cleaved caspase-3 in homogenates of ischemic cortex after 0h, 2h, 6h, 12h and 24h (n>5 per group). Caspase-3 activity was significantly differently from zero at 6h post-ischemia and increased progressively from then to reach its maximum value at 24h. The tubulin bands confirm equal loading. OD, optic density. Data represent mean ±SEM. Comparisons by t-test with control: *, $p < 0.05$; **, $p < 0.01$. **(C-H)** Expression and cellular distribution of cleaved caspase-3 and -9 in P12 ischemic cortex at 24h. Cells positive for cleaved caspase-3 **(C)** and -9 **(F)** are seen in the border of the lesion at 24h (arrows). By confocal microscopy, double labeling of cleaved caspase-3 **(D)** or cleaved caspase-9 **(G)** (red) with NeuN (green) reveals numerous colocalizations (yellow, arrowheads) whereas double labeling of cleaved caspase-3 **(E)** or -9 **(H)** (red) and GFAP (green) shows none. **(I-J)** Expression and cellular distribution of AIF in both control **(I)** and ischemic cortex at 24h **(J)**. Note that AIF is abundant in the nucleus following cerebral ischemia, unlike in the control. **(K-N)** Attempts at neuroprotection using the caspase inhibitors Z-VAD-fmk and Q-VD-OPH. **(K)** Quantification of cleaved caspase-3 in ischemic cortex homogenates of rats treated with saline or 500ng Z-VAD-fmk icv measured at 24h of reperfusion (n>5 per group). Z-VAD-fmk treatment strongly reduced the caspase-3 cleavage by 71.56% ± 9.08. **(L)** Lack of effect of post-ischemic Z-VAD-fmk administration (80, 160 or 500 ng icv) on brain injury at 24h. In no case did Z-VAD-fmk give neuroprotection (58.3±11.7, n=8, 59.7±9.4, n=5 and 60.8±11.0mm^3, n=5 for 80, 160 and 500ng-doses respectively) compared to saline (61±8.2mm^3, n=15). ANOVA showed no significant differences between the groups ($p = 0.9974$). **(M)** Quantification of cleaved caspase-3 in ischemic cortex homogenates from rats treated with saline, 1.3µg Q-VD-OPH icv, or 1mg/kg Q-VD-OPH ip at 24h of reperfusion (n>5 per group). Q-VD-OPH treatment strongly reduced the caspase-3 cleavage by 81.23% ± 3.05 (1.3µg, icv) or by 87.38% ± 6.36 (1mg/kg, ip). **(N)** Lack of effect of post-ischemic administration of Q-VD-OPH on brain injury in the same groups of rats as used for quantification of caspase cleavage. Q-VD-OPH injections did not provide significant neuroprotection, whether given icv (67.2±5.7mm^3, n=6) or ip (65.7±5.8mm^3, n=6) compared to saline (73.6±6.9mm^3, n=6). ANOVA showed no significant differences between the groups ($p = 0.638$). Bars: A = 5µm; C, F = 250µm; D, E, G, H = 100µm; I, J = 50µm.

Figure 2: Increase in autophagosomes after neonatal cerebral ischemia at P12.

(A) Upper panel: representative immunoblot of LC3 in extracts of ischemic cortex at 0h, 2h, 6h, 12h and 24h after reperfusion. Lower panel: quantification of the LC3-II band intensity expressed as a percentage of control LC3-II (n>5 per group), At 6h, the level of LC3-II in ischemic cortex had already reached 257% ± 32 of the control level, and at 24h was at 315% ± 27 of the control. Tubulin staining confirms equal loading. Data represent mean ±SEM. Comparisons by t-test with control: *, $p < 0.05$; **, $p < 0.01$. **(B-G)** Expression and distribution of LC3 after neonatal cerebral ischemia in P12 rats. Immunocytochemistry showed that LC3 labeling increased and appeared as numerous positive dots in the cytoplasm of cells in the ischemic area **(D, E)**, whereas non-ischemic brains displayed a less intense and more diffuse staining **(B, C)**. Double labeling for LC3 (red) and NeuN (green) of sections from the ischemic area demonstrated that LC3 is restricted to neuronal compartments (**F**, yellow), whereas double labeling for LC3 (red) and GFAP (green) showed no colocalization **(G)**. **(H)** Electron micrograph in the border of the lesion at 24h showing a neuron with numerous autophagosome-like structures (arrows) and autolysosomes containing membranous whorls (arrowheads). Bars: B, D = 50µm; C, E = 25µm; F, G = 50µm; H = 2µm.

Figure 3: Immunocytochemistry for cathepsin D (left) and LAMP1 (right) after cerebral ischemia in P12 rats.

Cathepsin D immunolabeling increased following cerebral ischemia from 6h **(B, B')** to 24h **(C, C')** as compared to control rat (unoperated) **(A, A')**. At high magnification **(B'-C')**, this enhancement is seen to reflect an increase in the number and size of cathepsin D positive cytosolic particles (presumably autolysosomes). Confocal microscopy of sections double labeled for cathepsin D (red) and NeuN (green) showed numerous colocalizations (**D, D'**, white arrows) whereas double labeling for cathepsin D (red) and GFAP (green) showed none **(E, E')**. LAMP1 immunocytochemistry showed enhanced LAMP1 staining from 6h **(G, G')** to 24h **(H, H')** post-ischemia as compared to control rat **(F, F')**. Double labeling and confocal microscopy for LAMP1 (**I**, red) and NeuN (**I'**, green) shows that increased LAMP1 expression is in NeuN positive cells (**I''**) whereas double labeling for LAMP1 (**J**, red) and GFAP (**J'**, green) shows no colocalization (**J''**). Bars: A-E, F-H, I-I'', J-J'' = 25µm; A'-C', F'-H' = 5µm; D'-E' = 10µm.

Figure 4: Acid phosphatase and β-hexosaminidase histochemistry and relationship between lysosomal and autophagosomal pathways after cerebral ischemia in P12 rats.

A strong increase in acid phosphatase staining is observed from 6h **(B)** to 24h post-reperfusion **(C)** in the ischemic area as compared to the control cortex **(A)**. At higher magnification, this enhancement is seen to involve an increase in the number of acid phosphatase positive dots at 6h **(B')** and in both their number and size at 24h **(C')** compared to control **(A')**. β-hexosaminidase histochemistry revealed a similar increase in staining from 6h **(E, E')** to 24h **(F, F')** post-ischemia as compared to control cortex **(D, D')**. At 24h, double labeling and confocal microscopy using cathepsin D and LC3 antibodies showed that the increase in cathepsin D (**G**, green) and LC3 (**G'**, red) occurred in the same neurons as demonstrated by numerous colocalizations (**G''**, yellow). Double labeling with LAMP1 (**H**, green) and LC3 (**H'**, red) also displayed numerous colocalizations (**H''**, yellow). Bars: A-C, D-F; G-G'': 50µm; H-H'': 25µm; A'-C', D'-F': 10µm.

Figure 5: Protective effect of 3-methyladenine treatment following cerebral ischemia at P12.

(A) Reduction of autophagy shown by Western blots for LC3-II. Saline (0.9% NaCl) or 3-methyladenine (3-MA) (60µg) solutions were injected icv at the time of reperfusion. Upper panel: representative immunoblot showing the effect of 3-MA on the autophagy marker LC3-II in extracts of ischemic cortex at 24h post-reperfusion. Lower panel: densitometric quantification of immunoreactive band intensities expressed as a percentage of control LC3-II (n>5 per group). 3-MA treatment almost completely inhibits the ischemia-dependent increase in LC3-II. Tubulin staining confirms equal loading. IL, ipsilateral; CL, contralateral; S, Saline. Data represent mean ±SEM. Comparisons by t-test with saline: *, $p < 0.05$; **, $p < 0.01$. **(B)** Effect of post-ischemic 3-MA administration on lesion volume at 24h. A single icv injection of 3-MA (60 µg) was performed at different times after reperfusion: 0h (n=9), 3h (n=7), 6h (n=6) compared to saline injected animals (n=9). 3-MA induced a substantial and significant reduction of the infarct volume when injected at 0h (34.6±6.0mm^3; p=0.009) or 3h (29.2±5.3mm^3; p=0.0015) post-ischemia as compared to saline (55.1±4.8mm^3), but not when injection occurred 6h after ischemia (53.4±8.2mm^3). Data represent mean ±SEM. Comparisons by t-test with saline: *, $p < 0.05$; **, $p < 0.01$. **(C-D)** Cresyl violet-stained sections showing representative brain injuries after icv injections of saline **(C)** or 3-MA 0h **(D)** at the level of the striatum and the hippocampus after 24h of reperfusion. Bar = 1mm. **(E, F)** Evaluation of the neuroprotective role of 3-MA in relation to the anterior to posterior distance. The neuroprotection was strongest at the level of the hippocampus, whether 3-MA was injected at 0h **(E)** or 3h **(F)** after reperfusion. Data represent mean ±SEM. Comparisons by t-test with saline: *, $p < 0.05$; **, $p < 0.01$.

Figure 6: Effect of 3-methyladenine treatment on nonautophagic modes of cell death after cerebral ischemia at P12.

Saline (0.9% NaCl) or 3-methyladenine (3-MA) (60µg) solutions were injected icv at the time of reperfusion. **(A)** Effect of 3-MA treatment on caspase-3 activation. Upper panel: Representative immunoblot of cleaved caspase 3 in extracts of ischemic cortex at 24h of reperfusion from rats treated with 3-MA or saline. Lower panel: Quantification of cleaved caspase 3 in the 3-MA-treated and saline-treated rats (n>5 per group). IL, ipsilateral; CL, contralateral. **(B)** Effect of 3-MA treatment on calpain activation. Upper panel: Representative immunoblot showing the calpain- and caspase-dependent fodrin cleavage products in extracts of ischemic cortex at 24h of reperfusion from rats treated with 3-MA or saline. IL, ipsilateral; CL, contralateral. Middle panel: Quantification of calpain-specific fodrin cleaved product (150 kDa) in the 3-MA and saline groups (n>5 per group). Lower panel: Quantification of caspase-specific fodrin cleaved product (120 kDa) in the 3-MA and saline groups (n>5 per group). Tubulin staining confirmed equal loading. Comparisons by t-test with saline: *, $p < 0.05$; **, $p < 0.01$. **(C)** Numbers of cells positive for cleaved caspase-9 per mm^2 in ischemic cortex at 24 h from rats treated with 3-MA ($109.7 \pm 19.4/mm^2$) or saline ($480.6 \pm 36.9/mm^2$). Data represent mean ±SEM. Comparisons by t-test with saline: *, $p < 0.05$; **, $p < 0.01$. **(D)** Numbers of AIF positive nuclei per mm^2 in ischemic cortex at 24 h from rats treated with 3-MA ($107.8 \pm 17.7/mm^2$) or saline. Data represent mean ±SEM. Comparisons by t-test with saline ($270 \pm 31.3/mm^2$). *, $p < 0.05$; **, $p < 0.01$.

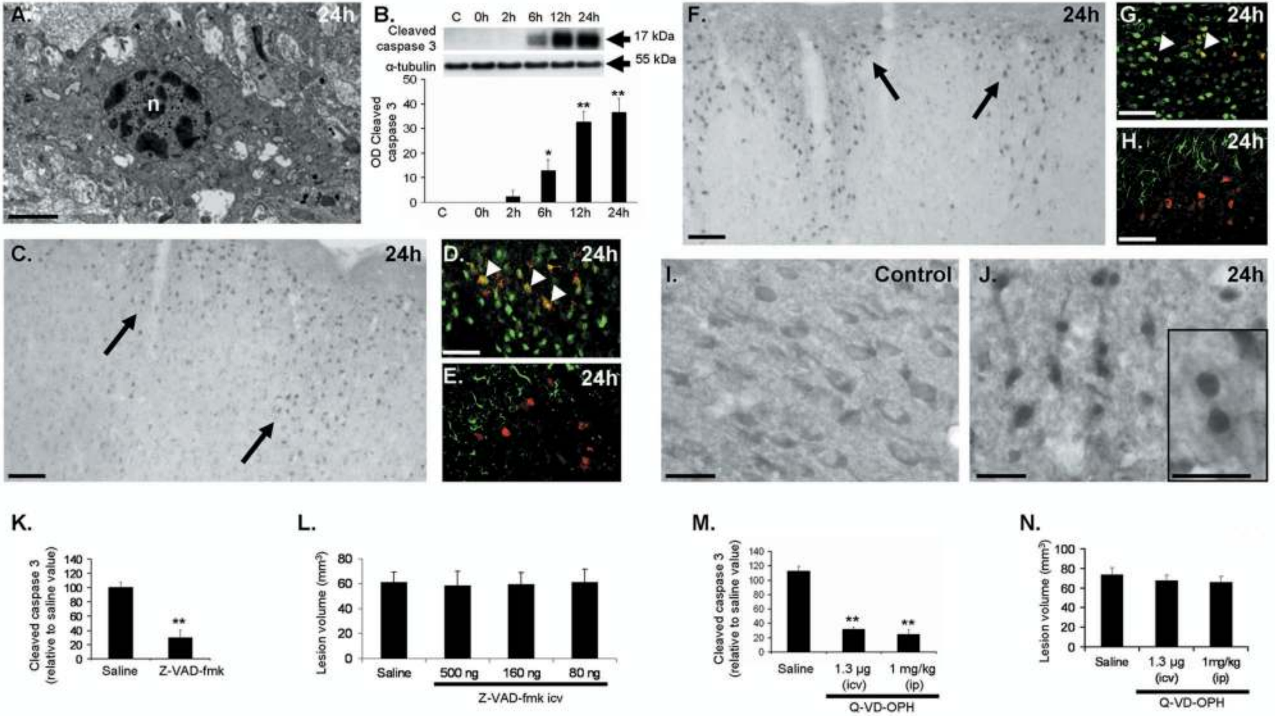

A.
24h
n
B.
C
0h
2h
6h
12h
24h
Cleaved caspase 3
α-tubulin
17 kDa
55 kDa
OD Cleaved caspase 3
C.
24h
D.
24h
E.
24h
F.
24h
G.
24h
H.
24h
I.
Control
J.
24h
K.
Cleaved caspase 3 (relative to saline value)
Saline
Z-VAD-fmk
L.
Lesion volume (mm³)
Saline
500 ng
160 ng
80 ng
Z-VAD-fmk icv
M.
Cleaved caspase 3 (relative to saline value)
Saline
1.3 µg (icv)
1 mg/kg (ip)
Q-VD-OPH
N.
Lesion volume (mm³)
Saline
1.3 µg (icv)
1mg/kg (ip)
Q-VD-OPH

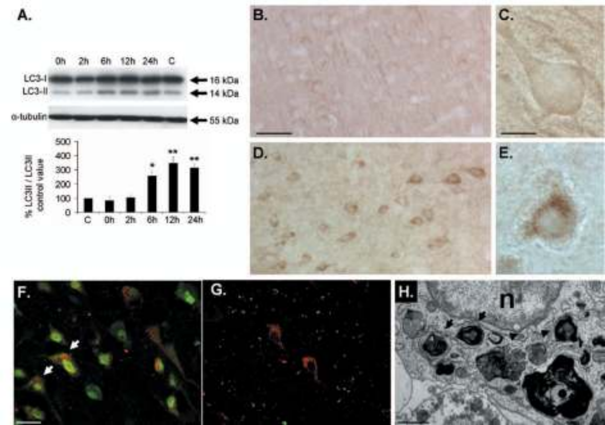

A.
0h
2h
6h
12h
24h
C
LC3-I
LC3-II
16 kDa
14 kDa
α-tubulin
55 kDa
% LC3II / LC3II control value
500
400
300
200
100
0
C
0h
2h
6h
12h
24h
*
**
**
B.
C.
D.
E.
F.
G.
H.
n

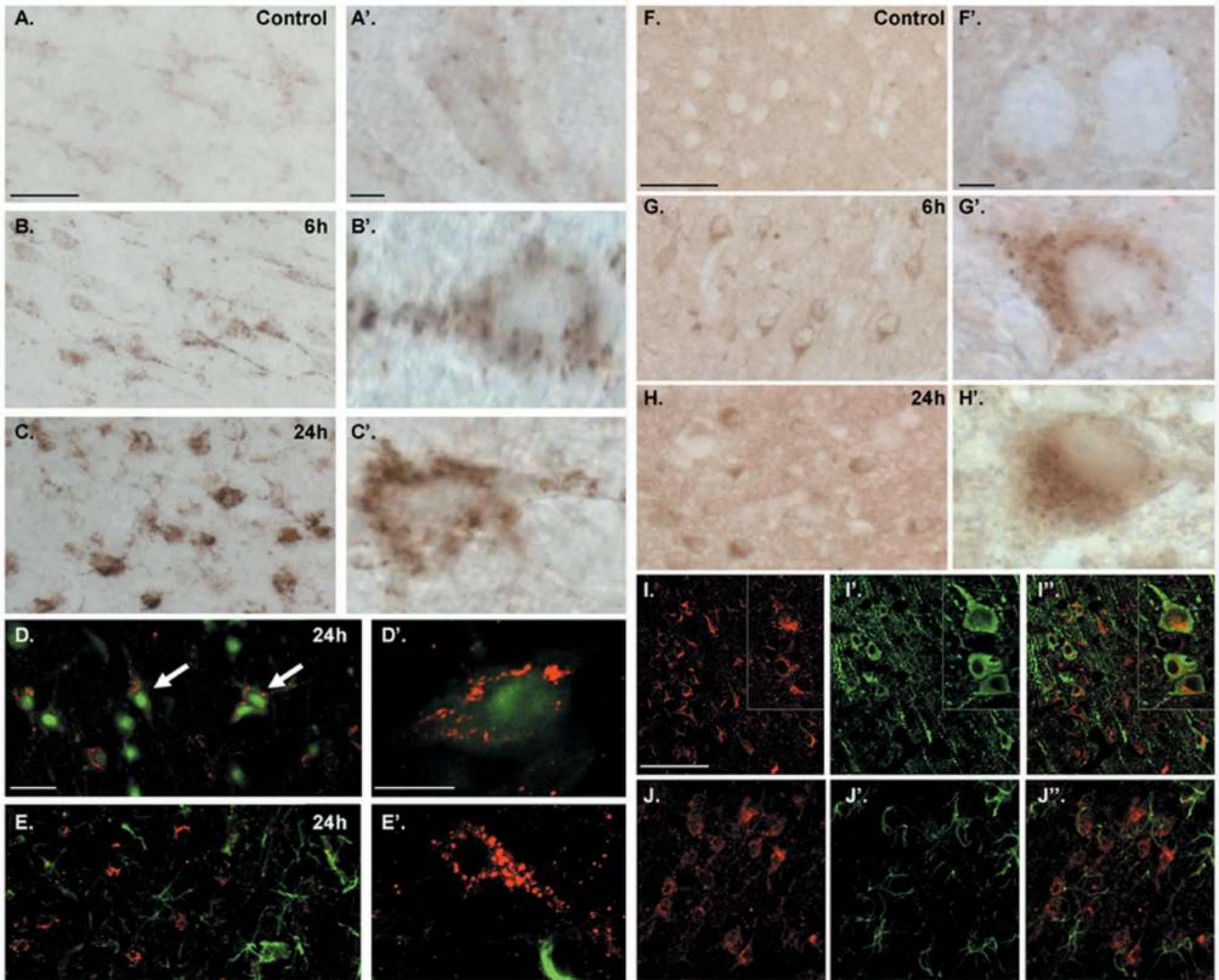

A.
Control
A'.
B.
6h
B'.
C.
24h
C'.
D.
24h
D'.
E.
24h
E'.
F.
Control
F'.
G.
6h
G'.
H.
24h
H'.
I.
I'.
I''.
J.
J'.
J''.

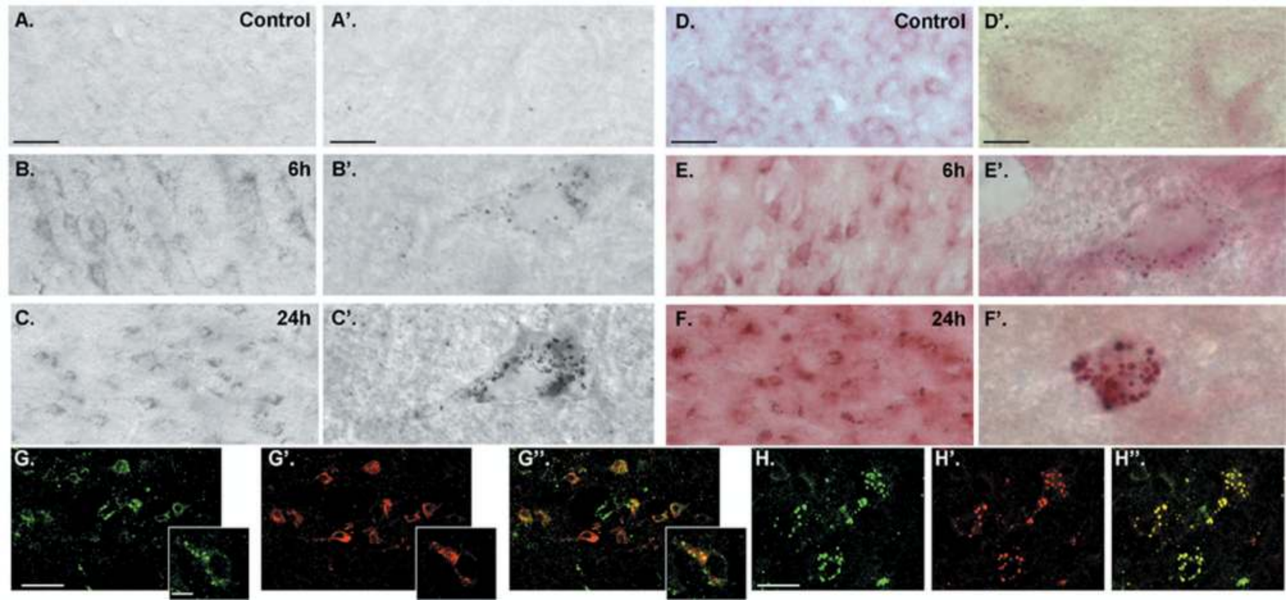
A.
Control
A'.
B.
6h
B'.
C.
24h
C'.
D.
Control
D'.
E.
6h
E'.
F.
24h
F'.
G.
G'.
G''.
H.
H'.
H''.

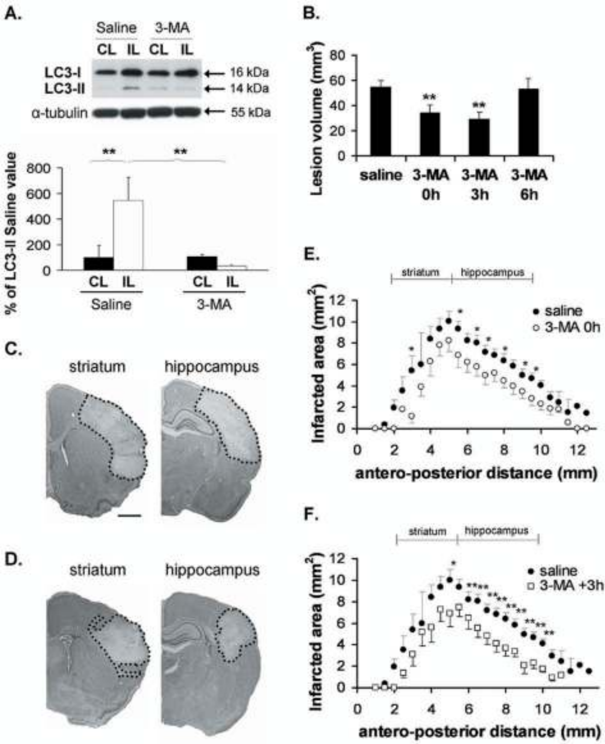
A.
Saline
3-MA
CL
IL
CL
IL
LC3-I
LC3-II
α-tubulin
16 kDa
14 kDa
55 kDa
**
**
% of LC3-II Saline value
800
600
400
200
0
CL
IL
CL
IL
Saline
3-MA
B.
Lesion volume (mm3)
80
60
40
20
0
**
**
saline
3-MA 0h
3-MA 3h
3-MA 6h
C.
striatum
hippocampus
D.
striatum
hippocampus
E.
striatum
hippocampus
Infarcted area (mm2)
saline
3-MA 0h
antero-posterior distance (mm)
F.
striatum
hippocampus
Infarcted area (mm2)
saline
3-MA +3h
antero-posterior distance (mm)

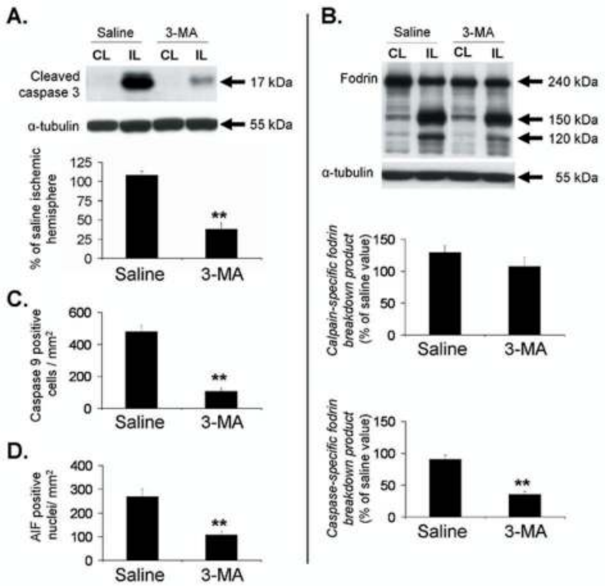

A.
Saline
3-MA
CL
IL
CL
IL
Cleaved caspase 3
17 kDa
α-tubulin
55 kDa
% of saline ischemic hemisphere
125
100
75
50
25
0
**
Saline
3-MA
B.
Saline
3-MA
CL
IL
CL
IL
Fodrin
240 kDa
150 kDa
120 kDa
α-tubulin
55 kDa
Calpain-specific fodrin breakdown product (% of saline value)
150
100
50
0
Saline
3-MA
Caspase-specific fodrin breakdown product (% of saline value)
150
100
50
0
**
Saline
3-MA
C.
Caspase 9 positive cells / mm2
600
400
200
0
**
Saline
3-MA
D.
AIF positive nuclei/ mm2
400
300
200
100
0
**
Saline
3-MA

Supplementary text for:

Post-ischemic treatment of neonatal cerebral ischemia should target autophagy

Julien Puyal, PhD, Anne Vaslin, PhD, Vincent Mottier and Peter G.H. Clarke, PhD

Supplementary Materials and Methods

Light microscopic immunocytochemistry

The rats were deeply anesthetized with pentobarbital (6mg/100mg body weight, Ip) and transcardially perfused (n >10 for each time) with 4% paraformaldehyde in 0.1M PBS, pH 7.4. The brain was rapidly dissected-out and post-fixed overnight at 4°C in the same fixative. Immunocytochemistry was carried out on both cryostat and vibratome coronal sections of the brain. For cryostat sections, the samples were immersed overnight in 30% sucrose in PBS at 4°C and frozen sections (18 µm) were collected on polylysine-coated slides. For vibratome sections, brains were washed thoroughly for 3h in PBS. Then 30-50 µm thick sections were cut on a Vibratome and collected serially in cold 0.1M PBS.

For fluorescence and confocal microscopy, sections were pre-incubated in PBS supplemented with 15% donkey serum and 0.3% Triton X-100 for 45 minutes at RT, and then incubated overnight at room temperature with the primary antibodies. All antibodies were diluted in PBS supplemented with 1.5%

donkey serum and 0.1% Triton X-100. The antibodies used were as follows: anti-MAP2 rabbit antibody (#AB5622, Millipore, Temacula, CA, USA), anti-NeuN mouse (#MAB377, Millipore, Temacula, CA, USA), anti-GFAP mouse (#G3893, Sigma, St. Louis, MO, USA), anti-S100β mouse (#S2532, Sigma, St. Louis, MO, USA), anti-LAMP1 mouse (#428017, Calbiochem, La Jolla, CA, USA) , anti-Cathepsin D rabbit (#06-467, Upstate, Charlottesville, VA, USA), anti-Cathepsin D goat (#sc-6486, Santa-Cruz Biotechnology, CA, USA), anti-LC3 rabbit (generous gift from Pr. Uchiyama), anti-AIF rabbit (#sc-5586, Santa-Cruz Biotechnology, CA, USA), anti-caspase 3 rabbit (#9661, Cell Signaling Technologies, Danvers, MA, USA), anti-caspase 9 rabbit (#9507, Cell Signaling Technologies, Danvers, MA, USA).

The sections were rinsed in PBS three times, for 10 minutes each, and then incubated with the secondary antibodies for 1 hour and 30 minutes: Alexa Fluor 594-labeled donkey IgGs or Alexa Fluor 488–labeled donkey anti-rabbit, anti-mouse or anti-goat IgGs (Molecular Probes, Eugene, OR, USA) depending on the first antibody. The sections were thoroughly rinsed in PBS and mounted in FluorSave (Calbiochem, San Diego, CA, USA). The sections were double-labeled, as above, by incubation with mixtures of poly- and monoclonal antibodies. The primary antibodies were detected with a mixture of Alexa Fluor 647-labeled anti-rabbit IgGs and Alexa Fluor 488-labeled anti-mouse IgGs, both diluted 1:200 in PBS. Control sections were incubated in the absence of primary antibodies. No specific immunofluorescence was detected for any of these controls. A LSM 510 Meta confocal microscope (Carl Zeiss, Thornwood, NY, USA) was used for confocal laser microscopy. Confocal images are displayed as individual optical sections. For double-labeling, immunoreactive signals were sequentially visualized in the same section with two distinct filters, with acquisition performed in separated mode. Images were processed with LSM 510 software and mounted using Adobe Photoshop.

For peroxidase revelation, endogenous peroxidase activity was blocked with 3% H_2O_2 in methanol for 20min. Primary antibodies were incubated as previously described followed by another 2h with a biotinylated donkey anti-mouse or donkey anti-rabbit or donkey anti-goat (Jackson Immunoresearch, West Grove, PA, USA) diluted 1:500 in PBS. Visualization was performed using Vectastain ABC Elite.

Cell counting

In different areas of ischemic cortex treated with saline ($n \geq 5$) or 3-MA ($n \geq 5$) at 24h post-ischemia, cells immunopositive for caspase-9, or containing AIF-positive nuclei, were counted at 20x magnification and expressed as an average number per mm^2. All data were expressed as mean ± SEM. Data were analyzed statistically by one-way ANOVA followed by Student's t-test (one-tailed, two-sample, and unequal variance). Unless specifically stated, ANOVA showed significant differences between the groups ($p < 0.05$).

Electron microscopy

At different times after ischemia, animals were anesthetized with pentobarbital

(6mg/100mg body weight, Ip) and perfused intracardially with fixative (2.5% glutaraldehyde and 2% paraformaldehyde) diluted in cacodylate buffer (0.1M, pH 7.4). The brain was rapidly dissected-out and post-fixed overnight at 4°C in the same fixative. Coronal vibratome sections (200-50µm thick) were cut and rinsed in cacodylate buffer. Sections were then postfixed in osmium tetroxide (1% in cacodylate buffer) for 30 min and contrasted in uranyl acetate (1% in ethanol 70%) for 5min. Sections were then dehydrated in graded alcohols and embedded in Durcarpan ACM resin (Fluka, Neu-Ulm, Germany) between silicon-coated glass slides. Regions of cortex were prepared and ultrathin sections (at a silver to gray interference) were cut with a diamond knife (Diatome). Sections were mounted on formvar-coated single slot grids. Sections were then contrasted with uranyl acetate and alkaline lead citrate. Sections were visualized using a Philips CM10 transmission electron microscope.

Western blots

Animals were killed by decapitation at different times after the beginning of the reperfusion (n>6 for each). Controls animals were killed on P13. The brains were rapidly dissected out in cold PBS containing 1mM $MgCl_2$, and the ipsilateral and contralateral cortices collected and homogenized in cold homogenization buffer: Hepes pH 7.4 20mM, NaCl 10mM, MgCl2 3mM, EGTA 2.5mM, DTT 0.1mM, NaF 50mM, Na3VO4 1mM, NP40 1% and freshly added complete EDTA-free anti-protease cocktail (Roche, cat.n°11873580001). Homogenization was performed gently by hand using a 2ml glass/glass homogenizer and the homogenate was sonicated and used for Western blotting.

The protein concentration of samples was determined using a Bradford assay and cell extracts were boiled for 3min in sodium dodecyl sulfate (SDS) buffer. The same quantities of proteins for each sample were resolved by SDS-PAGE (8%, 10% or 15% polyacrylamide) and transferred to a PVDF-membrane. After transfer, the membranes were blocked in 5% milk in TBS-T (Tris 200mM, NaCl 1.5M, Tween 20 0.1%) for 1h and incubated with the primary antibody in 5% milk in TBS-T overnight at 4°C. Anti-LC3 (#PD012, MBL, Naka-Ku Nagoya, Japan) was used at 1:1000, anti-cleaved caspase 3 was at 1:1000, anti-fodrin (#FG6090, Biomol international, Plymouth Meeting, PA, USA) at 1:1000 and anti-tubulin (#SC-8035, Santa-Cruz Biotechnology, CA, USA) at 1:5000. The membranes were washed, blocked in 1% milk in TBS-T for 30 min and incubated for 1h at RT with secondary horseradish peroxidase-coupled antibody (1:500, Pierce Biotechnology, Rockford, IL, USA) in 1% milk in TBS-T. After washes, immunoreactive products were detected by the enhanced chemiluminescence method. For reprobing, blots were stripped in SDS 2%, Tris 200mM, NaCl 1.5M and mercaptoethanol 100mM for 30 min at 60°C, washed with TBS and blocked again. The quantification of Western blots was performed using ImageQuant TL software (Amersham Biosciences) and values were normalized with respect to tubulin. The values were then expressed as a percentage relative to the control optical density (O.D) value. All data were expressed as mean ± SEM. Data were first verified to be normally distributed and then analyzed statistically by one-way ANOVA followed by Student's t-test (one-tailed, two-sample, and unequal variance). Unless specifically stated, ANOVA showed significant differences between the groups ($p < 0.05$).

Supplementary Results

Brain lesion characterization after focal cerebral ischemia in P12 rats

Focal cerebral ischemia was performed as previously described by Renolleau et al. (1998) with slight modifications. In the present study, the experiments were done in P12 rats and involved permanent occlusion of the middle cerebral artery followed by a transient (90 min) occlusion of the ipsilateral common carotid artery. The lesion was distinct and highly reproducible, being restricted mainly to the cortex but extending in some cases to the striatum. It started to be detectable at 5h after the beginning of the reperfusion (Suppl. Fig. S1A) and increased to reach its maximum value at 24h (Suppl. Fig. S1B), decreasing progressively thereafter to become a brain cavity as illustrated at the end of the first week (Suppl. Fig. S1C) and at P28 (Suppl. Fig. S1D).

We determined the spatio-temporal pattern of lesion development by measuring the cortical infarct area at different levels along the antero-posterior axis (Paxinos, 1988) at different times after reperfusion (Figure S1F). This revealed that the lesion developed fastest at the level of the striatum, and then spread caudally.

Necrosis occurred rapidly and was restricted to the center of the lesion

The presence of necrosis was investigated by both Western blot and electron microscopy. Western blots against fodrin were performed to investigate the involvement of calpain. The calpain-specific (150 kDa) band increased rapidly and lastingly after ischemic injury (Figure S2A, B). Already at the moment of reperfusion, it had almost tripled (289% ± 42) compared to control, and then it further increased to its maximum value at 12h (645% ± 86), thereafter remaining stable (647% ± 46 at 24h).

At the electron microscopic level, ultrathin sections of cortical regions localized in the center of the lesion showed dying neurons with necrotic morphology. At 24h after the beginning of reperfusion, dying neurons with swollen cell bodies (Figure S2F) and neurites (Figure S2G) were detected in the center of the lesion. These neurons displayed an increase in their cytoplasmic volume (but with loss of structured content), plasma membrane disruption (arrows) and at high magnification showed dilated organelles (such as mitochondria and endoplasmic reticulum) (Figure S2I) as compared to a control neuron (Figure S2D, E, H). However, there was little sign of chromatin condensation in the nucleus.

References

1. Renolleau S, Aggoun-Zouaoui D, Ben-Ari Y, Charriaut-Marlangue C. A model of transient unilateral focal ischemia with reperfusion in the P7 neonatal rat: morphological changes indicative of apoptosis. Stroke 1998;29:1454-60.
2. Paxinos G and Watson C. The Rat Brain in Stereotaxic Coordinates. New York: Academic Press,1982.

Supplementary figure legend

Figure S1: Evolution of the brain lesion over time following focal ischemia at P12.

Representative cresyl-violet stained coronal sections at the level of the hippocampus 5h **(A)**, 24h **(B)**, 7days **(C)** and 28 days **(D)** after reperfusion. Bar: 0.5 mm. **(E)** Lesion volume was assessed by measuring pale areas in cresyl violet-stained sections. Tissue loss was expressed in mm^3: 5h (13.6±5.8, n=5); 12h (37.7±10.4); 24h (55.1±4.8, n=9); 7 days (37.2±5.6, n=3); 14 days (23.5±13.3); 28 days (13.3±2.8, n=4). Data represent mean ±SEM. **(F)** Distribution of infarct area plotted as a function of anterior-to-posterior distance 5h, 12h and 24h after reperfusion. The increase in lesion volume occurred earlier in the more anterior parts.

Figure S2: Calpain involvement and necrosis following cerebral ischemia at P12.

(A) Representative immunoblot of calpain-dependent fodrin cleavage in ischemic cortex extracts after 0h, 2h, 6h, 12h and 24h of reperfusion. The tubulin bands confirm equal loading. **(B)** Quantification of calpain-specific fodrin cleaved product in homogenates of ischemic cortex after 0h, 2h, 6h, 12h and 24h (n>5 per group). The 150 kDa calpain-specific fodrin cleaved product showed a significant increase already at the moment of reperfusion (0h) and then increased progressively to reach its maximum value at 12h post-reperfusion. **(C)**

Quantification of caspase-specific fodrin cleaved product in the same homogenates after 0h, 2h, 6h, 12h and 24h (n>5/group). The 120 kDa caspase-3-specific fodrin breakdown product significantly increased from 6h to 24h after the beginning of the reperfusion. Data represents mean ±SEM. Comparisons by t-test with control (unoperated) rat cortex: *, $p < 0.05$; **, $p < 0.01$. **(D-I)** Electron micrographs showing the involvement of necrosis in the center of the lesion at 24h post-reperfusion but not in the non-ischemic hemisphere. Control neuron showing normal morphology of its cell body (including the nucleus, n) **(D)** and neurites **(E)**. **(H)** High magnification of control neuron's cytoplasm with mitochondria (m) and endoplasmic reticulum (er). Dying neuron located at the center of the lesion **(F)** and neurites **(G)**. High magnification of its cytoplasmic content **(I)**. Bars: D, F = 5µm; E, G = 1µm; H, **I** = 200nm.

Figure S3: Relationship between autophagic and apoptotic pathways after cerebral ischemia at P12.

Double labeling for cleaved caspase-3 (red; **A-D**) with LAMP1 (green; **A'-B'**) or cathepsin D (green; **C'** and **D'**) revealed no labeling for caspase-3 in cathepsin D or LAMP1 rich areas (**C''** and **B''**) and no labeling for cathepsin D or LAMP1 in caspase-3 rich areas (**A''** and **D''**). Double labeling for cleaved caspase-9 (red; **E-H**) with LAMP1 (green, **E'** and **F'**) or cathepsin D (green, **G'** and **H'**) likewise showed no colocalization in caspase-9 rich areas (**E''** and **G''**) or cathepsin D or LAMP1 rich areas (**G''** and **F''**). Confocal microscopy. Bars: 50µm.

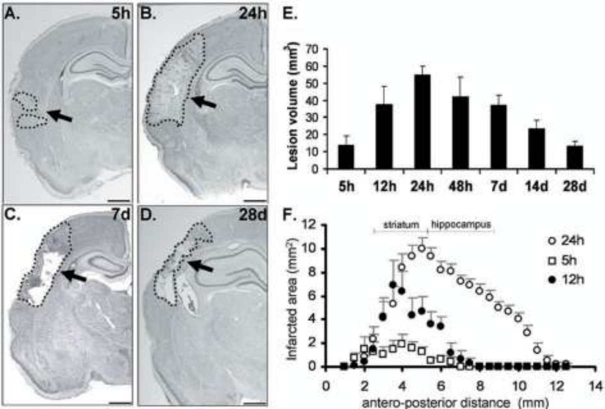

A.
5h
B.
24h
C.
7d
D.
28d
E.
Lesion volume (mm³)
70
60
50
40
30
20
10
0
5h
12h
24h
48h
7d
14d
28d
F.
Infarcted area (mm²)
12
10
8
6
4
2
0
striatum
hippocampus
24h
5h
12h
0
2
4
6
8
10
12
14
antero-posterior distance (mm)

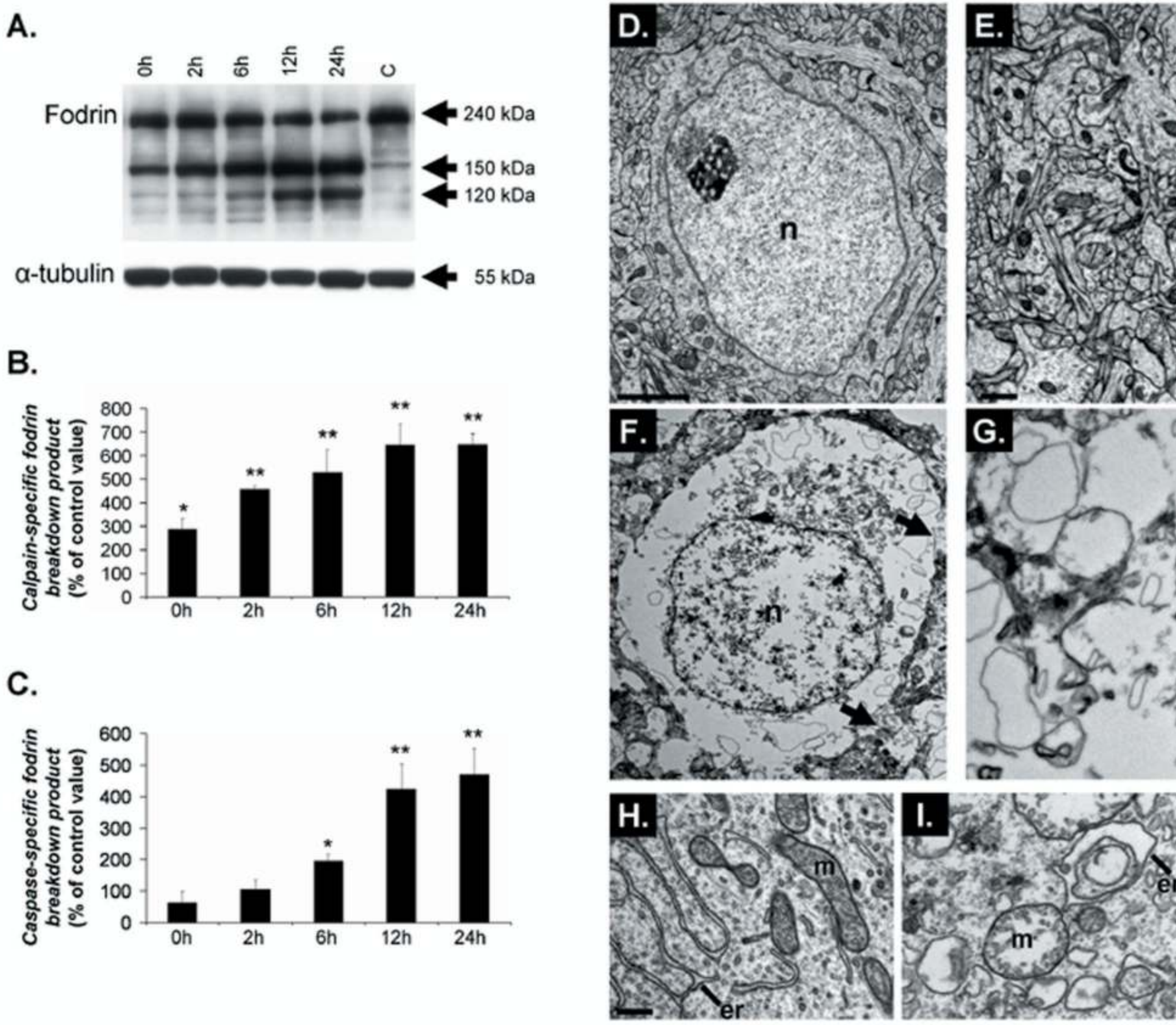

A.
0h
2h
6h
12h
24h
C
Fodrin
240 kDa
150 kDa
120 kDa
α-tubulin
55 kDa
B.
Calpain-specific fodrin breakdown product (% of control value)
800
700
600
500
400
300
200
100
0
0h
2h
6h
12h
24h
C.
Caspase-specific fodrin breakdown product (% of control value)
600
500
400
300
200
100
0
0h
2h
6h
12h
24h
D.
n
E.
F.
n
G.
H.
m
er
I.
m
er

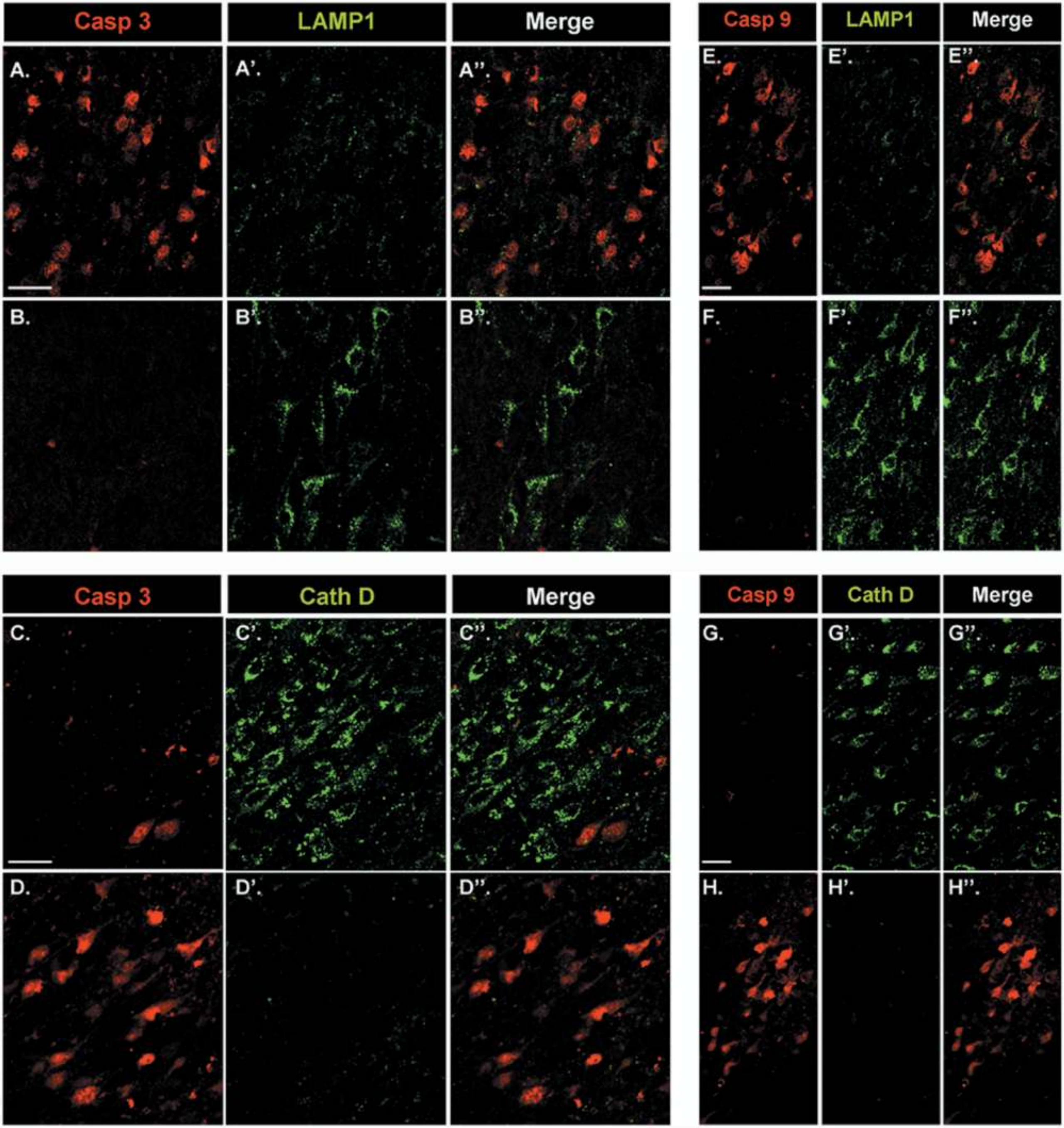

Casp 3
LAMP1
Merge
Casp 9
LAMP1
Merge
A.
A'.
A''.
E.
E'.
E''.
B.
B'.
B''.
F.
F'.
F''.
Casp 3
Cath D
Merge
Casp 9
Cath D
Merge
C.
C'.
C''.
G.
G'.
G''.
D.
D'.
D''.
H.
H'.
H''.